Mon. Not. R. Astron. Soc. **000**, 1–8 (2015) Printed 3 February 2015 (MN LATEX style file v2.2)

Connecting Faint End Slopes of the Lyman-α emitter and Lyman-break Galaxy Luminosity Functions

M. Gronke[1⋆], M. Dijkstra[1], M. Trenti[2,3], S. Wyithe[3,4]
[1] *Institute of Theoretical Astrophysics, University of Oslo, Postboks 1029, 0315 Oslo, Norway*
[2] *Kavli Institute for Cosmology and Institute of Astronomy, University of Cambridge, Cambridge, England*
[3] *School of Physics, University of Melbourne, Parkville, VIC 3010, Australia*
[4] *ARC Centre of Excellence for All-Sky Astrophysics (CAASTRO)*

3 February 2015

ABSTRACT

We predict Lyman-α (Lyα) luminosity functions (LFs) of Lyα-selected galaxies (Lyα emitters, or LAEs) at $z = 3{-}6$ using the phenomenological model of Dijkstra & Wyithe (2012). This model combines observed UV-LFs of Lyman-break galaxies (LBGs, or drop out galaxies), with constraints on their distribution of Lyα line strengths as a function of UV-luminosity and redshift. Our analysis shows that while Lyα LFs of LAEs are generally not Schechter functions, these provide a good description over the luminosity range of $\log_{10}(L_\alpha/\,\mathrm{erg\,s^{-1}}) = 41 - 44$. Motivated by this result, we predict Schechter function parameters at $z = 3 - 6$. Our analysis further shows that (*i*) the faint end slope of the Lyα LF is steeper than that of the UV-LF of Lyman-break galaxies, (with a median $\alpha_{Ly\alpha} < -2.0$ at $z \gtrsim 4$), and (*ii*) a turn-over in the Lyα LF of LAEs at Lyα luminosities 10^{40} erg s^{-1} $< L_\alpha \lesssim 10^{41}$ erg s^{-1} may signal a flattening of UV-LF of Lyman-break galaxies at $-12 > M_{\rm UV} > -14$. We discuss the implications of these results – which can be tested directly with upcoming surveys – for the Epoch of Reionization.

Key words: galaxies: high-redshift – galaxies: luminosity function, mass function – cosmology: reionization – ultraviolet: galaxies

1 INTRODUCTION

The luminosity function (LF) of galaxies provides one of the most basic statistical descriptions of a population of galaxies. It describes the number density of galaxies in a given luminosity interval. Generally, the LF is well described by a Schechter (1976) function

$$\phi(L)\mathrm{d}L = \phi^* \left(\frac{L}{L^*}\right)^\alpha \exp\left(-\frac{L}{L^*}\right) \mathrm{d}\left(\frac{L}{L^*}\right) \qquad (1)$$

with a normalization parameter ϕ^*, an exponential cutoff at $L \gtrsim L^*$, and, a power law with faint-end-slope α for $L \ll L^*$. The parameters depend on wavelength considered, galaxy type (e.g., passive versus star forming), and cosmic time.

At high redshift, galaxies are typically identified either through their broadband colors, for example using the drop-out or Lyman-break technique (Steidel et al. 1996), or through narrow-band searches aimed at detecting emission lines (Partridge & Peebles 1967; Djorgovski et al. 1985) In particular, young star forming galaxies emit a significant fraction of their radiation as Lyman-α (Lyα) emission, and this method has been proved to be very efficient in finding samples out to $z \sim 7$ (e.g. Rhoads et al. 2000; Rhoads & Malhotra 2001; Ouchi et al. 2008; Bond et al. 2009, 2010; Guaita et al. 2010; Kashikawa et al. 2011; Hibon et al. 2012; Ono et al. 2012; Ota & Iye 2012; Rhoads et al. 2012; Shibuya et al. 2012; Finkelstein et al. 2013; Konno et al. 2014).

Galaxies that have been selected (found) on the basis of their Lyα lines are referred to as 'Lyα emitters' (or LAEs). LAEs are useful because they are selected on having a strong Lyα line flux irrespective of their associated UV-continuum emission. Therefore, LAEs can be fainter in the continuum compared to Lyman-break galaxies, and complement galaxy samples obtained via broadband searches which have been extensively carried out with the Hubble Space Telescope out to $z \sim 10$ (e.g. Yan & Windhorst 2004; Beckwith et al. 2006; Bouwens et al. 2006; Wilkins et al. 2010; Trenti et al. 2011; Grazian et al. 2012; Finkelstein et al. 2012; Bouwens et al. 2014a; Finkelstein et al. 2014; Oesch et al. 2014; Schmidt et al. 2014). Moreover, the sensitivity of the observed Lyα flux to intervening neutral hydrogen gas makes LAEs an excellent probe of the Epoch of Reionization (see e.g. Dijkstra 2014, for a review).

⋆ E-mail: maxbg@astro.uio.no

Since the range of observed Lyα luminosities at high-z typically extends only over $\sim 1-1.5$ orders of magnitude, the shape of the Lyα LF is not strongly constrained and a fit with a Schechter function leads to significant degeneracy in the parameters. In particular the faint-end slope $\alpha_{\rm Ly\alpha}$ is essentially unconstrained: for example, Henry et al. (2012) used a sample of six (three) LAEs to find $\alpha_{\rm Ly\alpha}=-1.70^{+0.73}_{-0.57}$ ($\alpha_{\rm Ly\alpha}=-1.45^{+0.92}_{-0.70}$) at $z=5.7$. Other approaches include assuming a fixed value for $\alpha_{\rm Ly\alpha}$ and resorting to the data to constrain the other parameters (van Breukelen et al. 2005; Dawson et al. 2007; Ouchi et al. 2008; Hu et al. 2010; Kashikawa et al. 2011; Ciardullo et al. 2012; Zheng et al. 2013). In contrast, the ultraviolet (UV) LF of Lyman-break galaxies (LBGs) is much better constrained due to available data stretching over several orders of magnitude in luminosity (McLure et al. 2010; Yan et al. 2011; Bouwens et al. 2011; Bradley et al. 2012; Oesch et al. 2012; Yan et al. 2012; Lorenzoni et al. 2013; Schenker et al. 2013). For the faint end slope, the most recent by Bouwens et al. (2014a) finds $\alpha_{UV}=-1.91\pm0.09$ ($\alpha_{UV}=-1.64\pm0.04$) at $z\sim6$ ($z\sim4$).

There exists a clear opportunity to connect LAEs and LBGs via the Lyα line emission properties of LBGs. Shapley et al. (2003) provided a probability distribution function (PDF) of the rest-frame equivalent-width (EW) of the Lyα line in their sample of $\sim$ 800 $z\sim3$ LBGs. Dijkstra & Wyithe (2012) showed that this observed PDF was well described by an exponential function, and that the characteristic scale-length of this function *increased* towards fainter UV-luminosities. While there do not exist equally well measured PDFs at higher redshifts and/or fainter UV-luminosities, recent studies have constrained both the redshift and UV-luminosity dependence of the so-called 'Lyα fraction', which quantifies the fraction of LBGs for which the Lyα EW exceeds a certain value. The Lyα fractions – which represent integrated versions of the full EW PDF – increase from $z=2$ to $z=6$ at fixed $M_{\rm UV}$ (Stark et al. 2010; Cassata et al. 2015) and from UV-bright to UV-faint galaxies (Stark et al. 2010, 2011; Pentericci et al. 2011; Ono et al. 2012; Schenker et al. 2012).

There have been several attempts to link the redshift evolution of LBGs and their Lyα fractions to LAE luminosity functions (Dijkstra & Wyithe 2012; Faisst et al. 2014; Schenker et al. 2014). In this paper, we follow the work of Dijkstra & Wyithe (2012) and combine the most recent constraints on UV-LFs & Lyα fractions to make predictions for Lyα LFs. Dijkstra & Wyithe (2012) showed that this phenomenological model reproduces observed Lyα LFs and their redshift evolution remarkably well. Here, we focus specifically on the faint-end slope of the Lyα LF of LAEs, because (*i*) we can make robust predictions for this faint end slope, (*ii*) as we will show later, this faint end slope can be highly relevant for understanding the Epoch of Reionization.

This paper is structured as follows. In Sec. 2, we lay out our method. We present our results in Sec. 3 and discuss them in Sec. 4. Finally, we conclude in Sec. 5. The cosmological parameters we adopt are $\Omega_{\rm m}=0.3, \Omega_\Lambda=0.7, h=0.7, \sigma_8=0.9$.

2 METHOD

The number density of LAEs with luminosities in the interval $[L_\alpha \pm {\rm d}L_\alpha/2]$ is given by

$$\phi_{\rm LAE}(L_\alpha){\rm d}L_\alpha = {\rm d}L_\alpha F \int_{M_{UV,\rm min}}^{M_{UV,\rm max}} {\rm d}M_{UV}\, \phi(M_{UV}) P(L_\alpha|M_{UV}) \quad (2)$$

Here, $\phi(M_{UV}){\rm d}M_{UV}$ denotes the number density of LBGs as a function of in the range $M_{\rm UV}\pm{\rm d}M_{\rm UV}/2$. This function can be represented by the Schechter function with parameters $(\alpha_{UV}, M^*_{UV}, \phi^*_{UV})$.

The term $P(L_\alpha|M_{UV}){\rm d}L_\alpha$ is the conditional probability that a galaxy has a Lyα luminosity L_α given an absolute UV magnitude $M_{\rm UV}$. This conditional probability can be recast in terms of the equivalent width (EW) probability density function $P(EW|M_{UV})$ as $P(L_\alpha|M_{UV}) = P(EW|M_{UV})\frac{\partial EW}{\partial L_\alpha}$ if $EW > EW_{\rm LAE}$, where L_α and EW are related as $L_\alpha = EW L_\lambda = EW[\nu L_\nu/\lambda]$. Here, the luminosity/flux densities, frequency and wavelength are evaluated just longward of the Lyα resonance at $\lambda=(1216+\epsilon)$Å. We can extrapolate these flux/luminosities to their values where the UV-continuum measurements are usually made (see e.g. Dijkstra & Westra 2010)[1]. Furthermore, $EW_{\rm LAE}$ denotes the equivalent width threshold that determines whether a galaxy would make it into an LAE sample. We adopt that $EW_{\rm LAE}=0$Å, but note that some surveys adopt colour criteria for selecting LAEs as large as $EW_{\rm LAE}=64$Å (see Dijkstra & Wyithe 2012). If $EW \leqslant EW_{\rm LAE}$, then $P(L_\alpha|M_{UV})=0$ since in this case the galaxy does not qualify as an LAE. This threshold more closely represents detection threshold for Lyα emitting galaxies in spectroscopic surveys[2] – e.g., with *MUSE* (Bacon et al. 2010), *HETDEX* (Hill et al. 2008) and/or *VIMOS* (Cassata et al. 2011, 2015). We have verified that our main results do not depend on this choice[3].

The preceding factor F in Eq. (2) is merely a normalization constant to fit the data and, hence, can be thought of as the ratio of predicted versus the total number of LAEs. This factor should ideally be $F=1$. However, Dijkstra & Wyithe (2012) required that $F\sim0.5$. The origin of this number is not known (see Dijkstra & Wyithe 2012, for an extensive discussion)[4], but we stress it only affects the predicted normalization linearly and not the predicted faint-end slopes.

Hence, the key function in our analysis is $P(EW|M_{UV})$.

[1] We use the relation $L_\alpha = C_1 EW L_{UV,\nu}$ where $L_{UV,\nu}\propto\nu^{-\beta-2}$ is the UV luminosity density $L_{UV,\nu}$ and $C_1 \equiv \nu_\alpha/\lambda_\alpha(\lambda_{UV}/\lambda_\alpha)^{-\beta-2}$ converts the flux density at $\lambda=(1216+\epsilon)$Å to that at $\lambda_{UV}=1600$Å, which is the wavelength where $L_{UV,\nu}$ was measured (Dijkstra & Westra 2010).

[2] Note that in practise an EW cut is likely still needed to distinguish between LAEs and lower-z interlopers, such as [OII] emitters. This EW cut can nevertheless be lower than $EW_{\rm LAE}\sim20$Å (Leung et al. 2015)

[3] We have verified that varying $EW_{\rm LAE}$ in the range [0, 50] Å changes $\alpha_{\rm Ly\alpha}$ by ~0.02.

[4] The value of F depends weakly on the adopted UV Schechter function parameters. For example, Bowler et al. (2014) reported slightly different best-fit values, which drive F up to $F\sim0.7-0.8$. The Finkelstein et al. (2014) parameters, on the other hand, also suggest $F\sim0.5$.

Several functional forms have been explored in the literature. Schenker et al. (2014) compared the maximum likelihood values for several EW distributions to their *Keck MOSFIRE* (McLean et al. 2012) data, and concluded that the exponential distribution introduced by Dijkstra & Wyithe (2012) provides an adequate fit. This functional form is

$$P(EW|M_{UV},z) = \mathcal{N}\exp\left[-\frac{EW}{EW_c(M_{UV},z)}\right] \quad (3)$$

with $EW_c = EW_{c,0} + \mu_{M_{UV}}(M_{UV}+M_{UV,0}) + \mu_z(z+z_0)$ where $\mu_{M_{UV}}$, μ_z, $M_{UV,0}$, z_0, and $EW_{c,0}$ are model parameters. These parameters were chosen to match the observations of (Shapley et al. 2003) and Stark et al. (2010, 2011) as closely as possible. Furthermore, $\mathcal{N}$ is a normalization constant which is forced to be zero outside of $[EW_{\rm min}, EW_{\rm max}]$. Our choice of values for the model parameters is described in Sec. 3.3 where we present the numerical results. In Appendix A we show explicitly that the main results in this paper are insensitive to both the functional form of $P(EW)$ and the parameterization of EW_c.

3 RESULTS

We first present results in which $\rm EW_c$ =constant (in § 3.1). This allows us to demonstrate that for models in which the Lyα fraction does not evolve with $M_{\rm UV}$, the faint end slope of the LF of LAEs approaches that of LBGs. We then present a simplified model in § 3.2 in which the *mean* Lyα EW-PDF increases towards fainter UV-luminosity function. This model demonstrates quantitatively that the faint end slope of the LF of LAEs is steeper than that of LBGs if the Lyα fraction increases towards fainter UV-luminosities. In § 3.3 we present the results that we obtained from the EW-PDF given in Eq. (3).

3.1 Exemplary case with EW_c = const.

We consider the case $P(EW|M_{UV}) = P(EW)$, i.e. EW_c = const. $\equiv \lambda/C_1$. Furthermore, we set $\mathcal{N} = 0$ for $EW < EW_{\rm LAE}$. Under these assumptions we find

$$\phi(L_\alpha)\mathrm{d}L_\alpha \propto \int_0^\infty L_{UV,\nu}^{\alpha-1}\exp\left[-\frac{L_{UV,\nu}}{L^*_{UV}} - \frac{L_\alpha}{\lambda L_{UV,\nu}}\right]\mathrm{d}L_{UV,\nu} \quad (4)$$

$$\propto L_\alpha^{\alpha_{UV}/2}K_{-\alpha_{UV}}\left(2\sqrt{\frac{L_\alpha}{\lambda L^*_{UV}}}\right)\mathrm{d}L_\alpha \quad (5)$$

where $K_n(x)$ is the modified Bessel function of the second kind and L^*_{UV} is the luminosity corresponding to M^*_{UV}.

Eq. (5) shows that the Lyα LF generally does not take-on a Schechter form. The slope of the LF is given by

$$\alpha_{\rm Ly\alpha} \equiv \frac{\mathrm{d}\log\phi(L_\alpha)}{\mathrm{d}\log L_\alpha} = -\frac{\sqrt{y}K_{\alpha_{UV}-1}(2\sqrt{y})}{K_{\alpha_{UV}}(2\sqrt{y})} \quad (6)$$

with $y \equiv L_\alpha/(L^*_{UV}\lambda)$. For $L_\alpha \ll L^*_{UV}\lambda$ we have $y \ll 1$, and we obtain to leading order $\alpha_{\rm Ly\alpha} \approx -\Gamma(1-\alpha_{UV})/\Gamma(-\alpha_{UV}) = \alpha_{UV}$. Thus, having a *constant EW_c corresponds to an unchanged faint end slope, $a_{\rm Ly\alpha} = \alpha_{UV}$*.

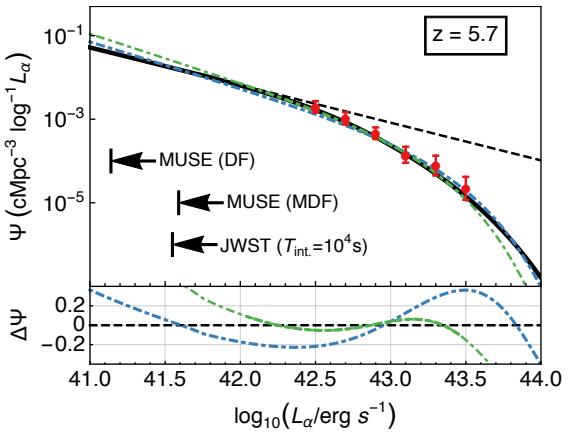

Figure 1. Upper panel: The predicted number of LAEs in the range $\log_{10}\left(L_\alpha/\,\mathrm{erg\,s^{-1}}\right) \pm \mathrm{d}\log_{10}\left(L_\alpha/\,\mathrm{erg\,s^{-1}}\right)$ using the UV LF evolution from Bouwens et al. (2014a) taken at $z = 5.7$ (black solid line). The grey dashed line marks the faint end slope ($\alpha_{\rm Ly\alpha} = -1.90$) and the dashed dotted lines show Schechter fits to our numerical findings. Once the fit was carried out over the whole shown luminosity range (blue) and once only in $\log_{10}(L/\,\mathrm{erg\,s^{-1}}) = [42, 43.5]$ (green). The red discs are the $z = 5.7$ observations by Ouchi et al. (2008) and the black arrows denote the *MUSE* deep field and medium deep field as well as the *JWST* limits at that redshift (see text for details). Lower panel: Relative deviation of the fits to the numerical results.

3.2 Exemplary case where $P(EW|M_{UV})$ evolves with M_{UV}

If EW_c depends on M_{UV} a general analytic solution for $\phi(L_\alpha)$ does not exist. For illustration purposes we first consider a case in which we replace Eq. (3) with a Dirac-δ distribution,

$$p(EW|L_{UV}) \propto \delta(EW - EW_d)\,, \quad (7)$$

where $EW_d(L_{UV}) \equiv EW_{d,0}\,(L_{UV}/L^*_{UV})^\gamma$. The parameter $\rm EW_d$ can be interpreted as the mean of the full PDF. This δ-function PDF leads[5] to

$$\phi(L_\alpha)\mathrm{d}L_\alpha \propto \mathrm{d}L_\alpha \times L_\alpha^{\alpha_{UV}/(\gamma+1)} \times \exp\left[-\left(\frac{L_\alpha}{C_1 EW_{d,0}L^*_{UV}}\right)^{1/(\gamma+1)}\right]. \quad (8)$$

Here, the faint end slope is $\alpha_{\rm Ly\alpha} = \alpha_{UV}/(\gamma+1)$. he Ly$\alpha$ LF thus has a *steeper* faint-end slope than the LBG LF, if $\gamma < 0$ (i.e. if EW_d decreases towards fainter $L_{\rm UV}$, as has been observed). Also note that we again obtain $\alpha_{\rm Ly\alpha} = \alpha_{UV}$ if EW_d does not evolve with $M_{\rm UV}$.

3.3 Realistic case with $P(EW|M_{UV})$ inferred from observations

For the model parameters of $P(EW|M_{\rm UV})$ in Eq. (3) we adopt the values from Dijkstra & Wyithe (2012)[6]. Example

[5] For simplicity, we set the minimum and maximum UV luminosity to zero and infinity, respectively.

[6] Specifically the model parameters related to EW_c are given by $(EW_{c,0}, \mu_{M_{UV}}, \mu_z, M_{\rm UV,0}, z_0, F)$ =

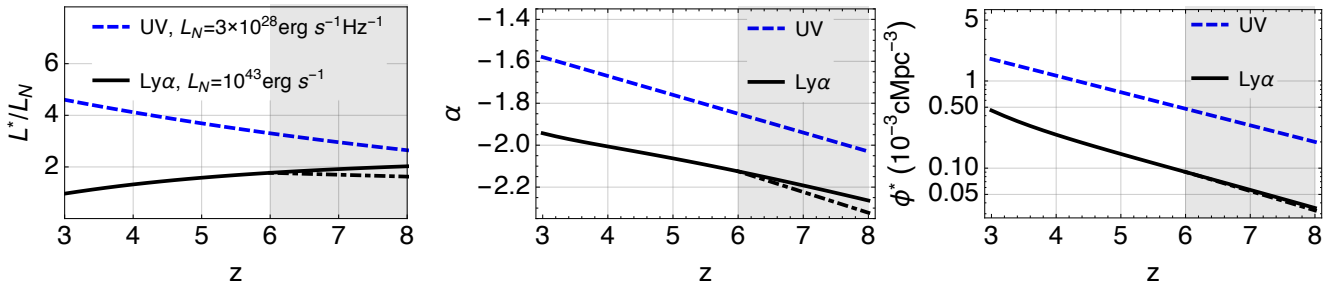

Figure 2. Evolution of the Schechter parameters of the UV LF from Bouwens et al. (2014a) (as *blue dashed lines*) and the parameters of the computed Lyα LF (*black lines*). In particular, the *left panel* shows the characteristic luminosity L^* (note the different normalization constants), the *central panel* the faint end slope α, and the *right panel* the overall normalization ϕ^*. Predictions at $z > 6$ (within the *shaded grey area*) do *not* account for reionization (see § 4.3). In this region, the *black solid lines* correspond to models with an uninterrupted EW evolution, whereas the *dashed-dotted lines* represent a model in which we freeze the EW evolution, i.e., $EW_c(z > 6) = EW_c(z = 6)$ (this assumption has been adopted in previous works).

EW-PDFs are shown in Appendix A1. For a more detailed motivation of this $P(EW)$ we refer the reader to Dijkstra & Wyithe (2012). We integrate the UV-LF over the range $M_{UV,(\mathrm{min,max})} = (-30, -12)$ when predicting Lyα luminosity functions, and discuss the impact of varying $M_{\max}$ in Sec. 4.

The redshift evolution of the best fit Schechter parameters of the UV LF is taken from Bouwens et al. (2014a) and given as $M^*_{UV} = -20.89 + 0.12z$, $\phi^*_{UV} = 0.48 \times 10^{-0.19(z-6)} 10^{-3}\mathrm{cMpc}^{-3}$, and, $\alpha_{UV} = -1.85 - 0.09(z-6)$. Following these analyses, we use $\lambda_{UV} = 1600\,\text{Å}$ as rest frame wavelength in which the UV continuum was measured and assume a UV spectral slope $\beta = -1.7$. This choice for β does not affect our results (see Appendix A4 for detailed discussion).

The upper panel of Fig. 1 shows the resulting number density of LAEs at $z = 5.7$ in the luminosity range $\log_{10} L_\alpha \pm \mathrm{d}\log_{10} L_\alpha/2$, i.e., $\psi(L_\alpha)\mathrm{d}\log_{10} L_\alpha$, as a function of L_α. This quantity is related to $\phi(L_\alpha)$ as $\psi(L_\alpha) = \phi(L_\alpha) L_\alpha \log 10$ ('log' denotes the natural logarithm). We compare these prediction to the data from Ouchi et al. (2008). In addition, we show the *MUSE* detection limits[7] for its medium deep field (MDF, limiting flux $F > 1.1 \times 10^{-18}\,\mathrm{erg\,s^{-1}cm^{-2}}$, integration time $T_{\mathrm{int.}} = 10\mathrm{h}$), and, deep field (DF, $F > 3.9 \times 10^{-19}\,\mathrm{erg\,s^{-1}cm^{-2}}$, $T_{\mathrm{int.}} = 80\mathrm{h}$) surveys as well as an exemplary *JWST*[8] limit ($F \gtrsim 10^{-18}\,\mathrm{erg\,s^{-1}cm^{-2}}$, $T_{\mathrm{int.}} = 10^4\,\mathrm{s}$).

Figure. 1 also shows two Schechter function approximations to our numerical findings fitted over the full luminosity-range shown (in *blue*) and over $\log_{10}(L_\alpha/\,\mathrm{erg\,s^{-1}}) = [40.5, 42]$ (in *green*). Although we do not expect the resulting Lyα LF to be a Schechter function (as shown in Sec. 3.2), it provides a reasonable fit over the displayed luminosity range.

(23 Å, 7 Å, 6 Å, 21.9, −4.0, 0.53). The EW-PDF covers the range $[EW_{\min}, EW_{\max}]$. Here, the lower limit $EW_{\min} \equiv -a_1$, where $a_1(M_{\mathrm{UV}})$ follows the form $a_1 = 20\,\text{Å}$ for $M_{UV} < -21.5$, $a_1 = (20 - 6(M_{UV} + 21.5)^2)\,\text{Å}$ for $-21.5 \leqslant M_{UV} \leqslant -19.0$ and $a_1 = -17.5\,\text{Å}$, otherwise (see Dijkstra & Wyithe 2012). We used $EW_{\max} = 1000\,\text{Å}$ but we verified that this choice does not affect our results quantitatively.

[7] *MUSE* survey limits taken from `http://muse.univ-lyon1.fr/IMG/pdf/science_case_gal_formation.pdf`.

[8] *JWST* survey limits obtained from `http://www.stsci.edu/jwst/science/sensitivity/`

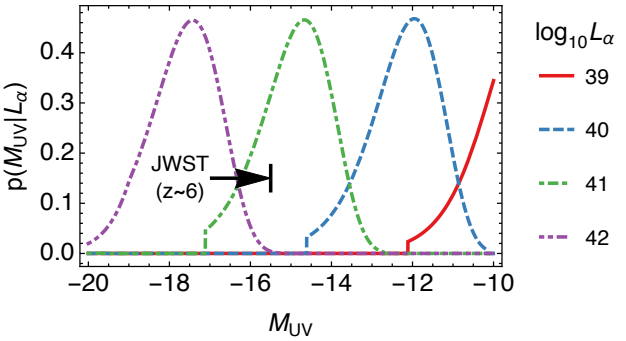

Figure 3. $p(M_{UV}|L_\alpha) \propto p(L_\alpha|M_{UV})\phi(M_{UV})$ versus M_{UV} for some exemplary values of L_α. The black arrow shows the *JWST* photometric limit quoted by Windhorst et al. (2006) for $z \sim 6$ which corresponds to $T_{\mathrm{int.}} \sim 10^6$ s integration time.

This can also be seen in the lower panel of Fig. 1, where we display the relative deviation of the fits to the LF.

Fig. 2 shows the redshift evolution of the Schechter best fit parameters (as *black lines*). Predictions for $z > 6$ do not account for reionization effects and are calculated with an unaltered EW evolution (solid line) as well as an EW-PDF which does not evolve after $z = 6$ (dash-dotted line). We discuss this result separately in § 4.3. For comparison, we plot the corresponding redshift parameterization of the UV LF by Bouwens et al. (2014a) (as *blue dashed lines*). The *left panel* shows that L^* increases by a factor ~ 2 over the redshift range $z = 3 - 6$, which differs from the redshift evolution in the characteristic UV-luminosity which drops by 20%. This difference is driven by the redshift evolution in the Lyα EW-PDF, which in turn was inferred from the observed redshift-evolution of Lyα 'fractions' over this redshift range. The *central panel* shows that $\alpha_{\mathrm{Ly}\alpha} < \alpha_{UV}$. This is again a consequence of inferred redshift evolution of the Lyα-EW PDF (see § 3.2). This figure also illustrates the close-to-linear $\alpha_{\mathrm{Ly}\alpha}$–$z$ relation. This evolution is mostly driven by the redshift evolution of α_{UV}. Finally, the *right panel* shows the predicted redshift evolution in ϕ^*.

4 DISCUSSION

4.1 Low-L turnover

The integral over $\phi(L_\alpha)\mathrm{d}L_\alpha$ diverges for $\alpha < -2$. We therefore expect that the luminosity function flattens or turns-over below some luminosity. The minimum luminosity that we can account for in our models is

$$L_{\alpha,\mathrm{min}} = EW_{\mathrm{min}}(M_{\mathrm{UV,max}})\ C_1 L_{\mathrm{UV,min}}, \qquad (9)$$

where $EW_{\mathrm{min}} = -a_1 = 17.5\,\text{Å}$ (see footnote 6 in § 3.3) denotes the minimum equivalent width in our EW-PDF at the maximum absolute UV-magnitude (i.e. the lowest UV-luminosity). For example, we obtain $L_{\alpha,\mathrm{min}} \sim 10^{39}\,\mathrm{erg\,s^{-1}}$ for $M_{\mathrm{UV,max}} = -12$. At this luminosity we expect the predicted Lyα luminosity to go to zero, as is shown in Figure 4.

An estimate for where we may start to see departures from a power-law slope can be obtained by considering the conditional probability $p(M_{UV}|L_\alpha)$. Bayes' theorem states that $p(M_{UV}|L_\alpha) \propto \phi(L_\alpha|M_{UV})\phi(M_{UV})$, of which we show examples in Fig. 3 for four different values of L_α. This Figure illustrates for example that Lyα observations that probe a flux corresponding to $L_\alpha = 10^{40}$ erg s^{-1} – a level that can be reached in *MUSE* ultra deep fields – effectively probe galaxies with $-14 < M_{\mathrm{UV}} < -11$, which are fainter than can be probed directly even with the *JWST*. The *JWST* detection limit shown in Figure 3 is taken from Windhorst et al. (2006). Figure 3 further shows that if the UV-LF flattens off at – say – $M_{\mathrm{UV}} \gtrsim -12$ that then the effects should become noticeable in the predicted Lyα luminosity function around $L_\alpha = 10^{40}$ erg s^{-1}, as here galaxies with $M_{\mathrm{UV}} \sim -12$ dominate the contribution to the Lyα LF.

In Figure 4 we make these points more explicit, and show the predicted faint end of the LAE LF for four values of $M_{UV,\mathrm{max}}$ (calculated with the UV LF parameters at $z = 3.1$). For each curve we marked $L_{\alpha,\mathrm{min}}$ with *dotted lines*. For example, a potential UV turnover at $M_{UV} \sim -12$ leads to deviations[9] of the Lyα LF at $L_\alpha \sim 10^{40}\,\mathrm{erg\,s^{-1}}$ and a cut-off at $L_\alpha \sim 10^{39}\,\mathrm{erg\,s^{-1}}$. Figure 4 also contains data points taken from Rauch et al. (2008). Rauch et al. (2008) performed an ultra deep (92-hr) exposure with *VLT*s *FORS2* low resolution spectrograph. The goal of these observations was to detect fluorescent Lyα emission from optically thick clouds powered by the ionizing background. While their sensitivity turned out not to be good enough to detect this fluorescent emission (revised estimates of the ionizing background and the conversion efficiency into Lyα), they detected numerous ultra faint Lyα emitting sources characterizing their LF down to $L_\alpha \sim 6 \times 10^{40}\,\mathrm{erg\,s^{-1}}$. We computed the uncertainties with the cosmic variance calculator of Trenti & Stiavelli (2008). These data-points fall on the predicted LF for $M_{\mathrm{UV,max}} = -16$. However we caution that the turn-over occurs at the lowest luminosity data-point only, which might suffer from incompleteness (although it lies above the detection threshold). In the same figure we provide the estimated *MUSE* limits for the deep field (DF) and the gravitationally lensed ultra deep field (UDF) surveys.

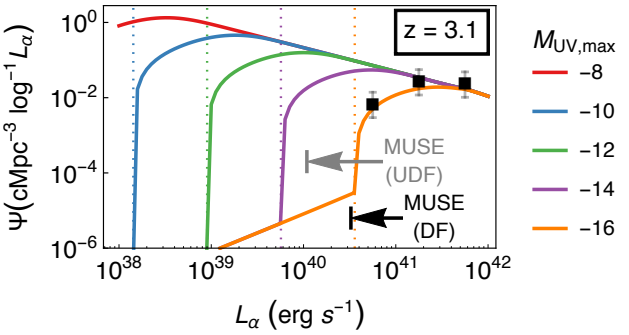

Figure 4. $\psi(L_\alpha)\mathrm{d}L_\alpha$ versus L_α at $z = 3.1$ for different values of $M_{UV,\mathrm{max}}$ illustrating the cutoff at low Lyα luminosities. The dashed and dotted lines show the "cutoff" and "deviation" points for each $M_{UV,\mathrm{max}}$ discussed in Sec. 4. Data points are from Rauch et al. (2008) taken at that redshift (see the text for a discussion on the error bars). And the black (grey) arrow denotes planned future *MUSE* (ultra) deep field limits.

4.2 Implications for the Epoch of Reionization

Low luminosity galaxies are expected to play a major role in driving the reionization of the Universe (e.g. Robertson et al. 2010; Trenti et al. 2010; Kuhlen & Faucher-Giguère 2012; Boylan-Kolchin et al. 2014). Determining the faint end of the LF such as its slope and a turnover luminosity is essential for constraining the volume emissivity of ionizing photons. However, even future experiments will have difficulties detecting these galaxies directly via their UV continuum flux. Current constraints rely, therefore, on extrapolation of local properties to higher redshifts (Weisz et al. 2014), (relatively few) gravitationally lensed objects (Alavi et al. 2014; Atek et al. 2014) or inferences from gamma-ray burst observations (Trenti et al. 2012). In this work, we have shown that the Lyα LF can provide an independent probe of the faint end of the UV LF, and that for example the *MUSE* DF survey could already detect (or rule out) a turnover at $M_{UV} \lesssim -15$.

Recent studies have shown that Lyα escape may be correlated with the escape of ionizing photons (Behrens et al. 2014; Verhamme et al. 2014), as the escape of ionizing photons requires low HI-column density ($N_{\mathrm{HI}} < 10^{17}$ cm^{-2}) channels, which can also provide escape routes for Lyα photons. The fact that Lyα LFs are likely steeper than the UV LFs implies that the Lyα volume emissivity – and therefore possibly the ionizing emissivity – are weighted more strongly towards low luminosity galaxies. This is consistent with the expectation that ionizing photons escape more easily from lower mass – and hence lower luminosity – galaxies. A steep faint-end slope of the Lyα LF may therefore provide observational support for this scenario.

4.3 Predictions for redshifts $z = 6 - 8$

We extrapolated our predictions for the best-fit Schechter parameters of the LAE LF to $z > 6$ in two ways (shown in Fig. 2): *(i)* in the first, we assume that the EW-PDF continues to evolve as inferred from the observations at $z = 3 - 6$.

[9] The first deviations in the Lyα LF can be found at $L_{\alpha,\mathrm{dev.}} = C_1 L_{UV}(x) EW_c(x)$ with $x \equiv M_{UV,\mathrm{max}} - \Delta M_{UV}$. Here, ΔM_{UV} describes the half width of $p(M_{UV}|L_\alpha)$ at a chosen probability threshold.

This model is represented by the *solid lines*, and, *(ii)* in the second, we 'freeze' the EW distribution for $z > 6$ at the value it had at $z = 6$ (*dashed lines*). This latter assumption has been common in previous works (see e.g. Dijkstra et al. 2011; Bolton & Haehnelt 2013; Jensen et al. 2013; Choudhury et al. 2014; Mesinger et al. 2015). We show results for these two models to get a sense for the uncertainties on our predictions. We stress that we have purposefully *not* modelled the impact of reionization on the EW-PDF. Reionization is likely responsible for the observed 'drop' in the observed Lyα fractions at $z > 6$ (e.g. Pentericci et al. 2011; Schenker et al. 2012; Ono et al. 2012; Treu et al. 2013; Caruana et al. 2014; Tilvi et al. 2014). Understanding this drop has been the main focus of previous works, and is outside the scope of this paper. Our predictions for $z = 6 - 8$ are useful in a different way, as they provide predictions for the Lyα LFs of LAEs in the absence of reionization. Comparison to observed LFs at these redshifts highlight the impact of reionization.

5 CONCLUSIONS

We predicted Lyα luminosity functions (LFs) of Lyα-selected galaxies (Lyα emitters, or LAEs) at $z = 3 - 6$ using the phenomenological model of Dijkstra & Wyithe (2012). This model combines observed UV-LFs of Lyman-break galaxies (LBGs), with observational constraints on the Lyα EW PDF of these LBGs, as a function of $M_{\rm UV}$ and redshift. The results from our analysis can be summarized as follows:

- While Lyα luminosity functions of LAEs are generally not Schechter functions, these provide a good description over the luminosity range of $\log_{10}(L_\alpha/\,{\rm erg\,s^{-1}}) = 41 - 44$ (see Fig. 1).
- We predict Schechter function parameters at $z = 3 - 6$ (shown in Fig. 2). The faint end slope of the Lyα LF is steeper than that of the UV-LF of LBGs, with a median $\alpha_{Ly\alpha} < -2.0$ at $z \gtrsim 4$ (see the *central panel* in Fig. 2). While the current work was in the advanced stage of completion, Dressler et al. (2014) posted a preprint in which they observationally infer a very steep faint end slope at $z \sim 5.7$ ($-2.35 < \alpha < -1.95$, also see Dressler et al. (2011)). The central value $\alpha = -2.15$ is in excellent agreement with the value $\alpha \sim -2.1$ predicted in our framework.
- The faint end of the LAE LF provides independent constraints on the very faint end of the UV-LF of LBGs. For example, the predicted LAE LF at Lyα luminosities 10^{40} erg s^{-1} $< L_\alpha \lesssim 10^{41}$ erg s^{-1} is sensitive to the UV-LF of LBGs in the range $-11 > M_{\rm UV} > -15$ (see Fig. 3 and Fig. 4). These LBGs are too faint to be detected directly (even with JWST). A turn-over in the Lyα LF of LAEs may signal a flattening of UV-LF of LBGs. We discuss implications of these results for the Epoch of Reionization in § 4.2.

We have verified that these results are insensitive to our assumed functional form of $P(EW)$ and how we parameterized its dependence on z and $M_{\rm UV}$. Our predictions can be tested directly with various upcoming surveys.

ACKNOWLEDGEMENTS

We thank Masami Ouchi for kindly providing the data points shown in Fig. 1. MD and MT thank Alan Dressler giving a presentation which inspired this work at the UCSB GLASS meeting in May 2014.

REFERENCES

Alavi A., et al., 2014, ApJ, 780, 143
Atek H., et al., 2014, ApJ, 786, 60
Bacon R., et al., 2010, in Society of Photo-Optical Instrumentation Engineers (SPIE) Conference Series. , doiXX:10.1117/12.856027
Beckwith S. V. W., et al., 2006, AJ, 132, 1729
Behrens C., Dijkstra M., Niemeyer J., 2014, preprint (arXiv:1401.4860)
Bolton J. S., Haehnelt M. G., 2013, MNRAS, 429, 1695
Bond N. A., Gawiser E., Gronwall C., Ciardullo R., Altmann M., Schawinski K., 2009, ApJ, 705, 639
Bond N. A., Feldmeier J. J., Matković A., Gronwall C., Ciardullo R., Gawiser E., 2010, ApJ, 716, L200
Bouwens R. J., Illingworth G. D., Blakeslee J. P., Franx M., 2006, ApJ, 653, 53
Bouwens R. J., et al., 2011, ApJ, 737, 90
Bouwens R. J., et al., 2014a, preprint (arXiv:1403.4295)
Bouwens R. J., et al., 2014b, ApJ, 793, 115
Bowler R. A. A., et al., 2014, ArXiv e-prints,
Boylan-Kolchin M., Bullock J. S., Garrison-Kimmel S., 2014, MNRAS, 443, L44
Bradley L. D., et al., 2012, ApJ, 760, 108
Caruana J., Bunker A. J., Wilkins S. M., Stanway E. R., Lorenzoni S., Jarvis M. J., Ebert H., 2014, MNRAS, 443, 2831
Cassata P., et al., 2011, A&A, 525, A143
Cassata P., et al., 2015, A&A, 573, A24
Choudhury T. R., Puchwein E., Haehnelt M. G., Bolton J. S., 2014, preprint (arXiv:1412.4790),
Ciardullo R., et al., 2012, ApJ, 744, 110
Dawson S., Rhoads J. E., Malhotra S., Stern D., Wang J., Dey A., Spinrad H., Jannuzi B. T., 2007, ApJ, 671, 1227
Dijkstra M., 2014, PASA, 31, 40
Dijkstra M., Westra E., 2010, MNRAS, 401, 2343
Dijkstra M., Wyithe J. S. B., 2012, MNRAS, 419, 3181
Dijkstra M., Mesinger A., Wyithe J. S. B., 2011, MNRAS, 414, 2139
Djorgovski S., Spinrad H., McCarthy P., Strauss M. A., 1985, ApJ, 299, L1
Dressler A., Martin C. L., Henry A., Sawicki M., McCarthy P., 2011, ApJ, 740, 71
Dressler A., Henry A., Martin C. L., Sawicki M., McCarthy P., Villaneuva E., 2014, preprint (arXiv:1412.0655),
Faisst A. L., Capak P., Carollo C. M., Scarlata C., Scoville N., 2014, ApJ, 788, 87
Finkelstein S. L., et al., 2012, ApJ, 756, 164
Finkelstein S. L., et al., 2013, Nature, 502, 524
Finkelstein S. L., et al., 2014, preprint (arXiv:1410.5439),
Grazian A., et al., 2012, A&A, 547, A51
Guaita L., et al., 2010, ApJ, 714, 255
Henry A. L., Martin C. L., Dressler A., Sawicki M., McCarthy P., 2012, ApJ, 744, 149

Hibon P., Kashikawa N., Willott C., Iye M., Shibuya T., 2012, ApJ, 744, 89
Hill G. J., et al., 2008, in Kodama T., Yamada T., Aoki K., eds, Astronomical Society of the Pacific Conference Series Vol. 399, Panoramic Views of Galaxy Formation and Evolution. p. 115, arXiv:0806.0183
Hu E. M., Cowie L. L., Barger A. J., Capak P., Kakazu Y., Trouille L., 2010, ApJ, 725, 394
Jensen H., Laursen P., Mellema G., Iliev I. T., Sommer-Larsen J., Shapiro P. R., 2013, MNRAS, 428, 1366
Kashikawa N., et al., 2011, ApJ, 734, 119
Konno A., et al., 2014, preprint (arXiv:1404.6066),
Kuhlen M., Faucher-Giguère C.-A., 2012, MNRAS, 423, 862
Leung A. S., Gawiser E. J., Acquaviva V., Hetdex Collaboration 2015, in American Astronomical Society Meeting Abstracts. p. 336.49
Lorenzoni S., Bunker A. J., Wilkins S. M., Caruana J., Stanway E. R., Jarvis M. J., 2013, MNRAS, 429, 150
McLean I. S., et al., 2012, in Society of Photo-Optical Instrumentation Engineers (SPIE) Conference Series. , doiXX:10.1117/12.924794
McLure R. J., Dunlop J. S., Cirasuolo M., Koekemoer A. M., Sabbi E., Stark D. P., Targett T. A., Ellis R. S., 2010, MNRAS, 403, 960
Mesinger A., Aykutalp A., Vanzella E., Pentericci L., Ferrara A., Dijkstra M., 2015, MNRAS, 446, 566
Oesch P. A., et al., 2012, ApJ, 759, 135
Oesch P. A., et al., 2014, ApJ, 786, 108
Ono Y., et al., 2012, ApJ, 744, 83
Ota K., Iye M., 2012, MNRAS, 423, 444
Ouchi M., et al., 2008, ApJS, 176, 301
Partridge R. B., Peebles P. J. E., 1967, ApJ, 147, 868
Pentericci L., et al., 2011, ApJ, 743, 132
Rauch M., et al., 2008, ApJ, 681, 856
Rhoads J. E., Malhotra S., 2001, ApJ, 563, L5
Rhoads J. E., Malhotra S., Dey A., Stern D., Spinrad H., Jannuzi B. T., 2000, ApJ, 545, L85
Rhoads J. E., Hibon P., Malhotra S., Cooper M., Weiner B., 2012, ApJ, 752, L28
Robertson B. E., Ellis R. S., Dunlop J. S., McLure R. J., Stark D. P., 2010, Nature, 468, 49
Schechter P., 1976, ApJ, 203, 297
Schenker M. A., Stark D. P., Ellis R. S., Robertson B. E., Dunlop J. S., McLure R. J., Kneib J.-P., Richard J., 2012, ApJ, 744, 179
Schenker M. A., et al., 2013, ApJ, 768, 196
Schenker M. A., Ellis R. S., Konidaris N. P., Stark D. P., 2014, ApJ, 795, 20
Schmidt K. B., et al., 2014, ApJ, 786, 57
Shapley A. E., Steidel C. C., Pettini M., Adelberger K. L., 2003, ApJ, 588, 65
Shibuya T., Kashikawa N., Ota K., Iye M., Ouchi M., Furusawa H., Shimasaku K., Hattori T., 2012, ApJ, 752, 114
Stark D. P., Ellis R. S., Chiu K., Ouchi M., Bunker A., 2010, MNRAS, 408, 1628
Stark D. P., Ellis R. S., Ouchi M., 2011, ApJ, 728, L2
Steidel C. C., Giavalisco M., Pettini M., Dickinson M., Adelberger K. L., 1996, ApJ, 462, L17
Tilvi V., et al., 2014, ApJ, 794, 5
Trenti M., Stiavelli M., 2008, ApJ, 676, 767
Trenti M., Stiavelli M., Bouwens R. J., Oesch P., Shull J. M., Illingworth G. D., Bradley L. D., Carollo C. M., 2010, ApJ, 714, L202
Trenti M., et al., 2011, ApJ, 727, L39
Trenti M., Perna R., Levesque E. M., Shull J. M., Stocke J. T., 2012, ApJ, 749, L38
Treu T., Schmidt K. B., Trenti M., Bradley L. D., Stiavelli M., 2013, ApJ, 775, L29
Verhamme A., Orlitova I., Schaerer D., Hayes M., 2014, preprint (arXiv:1404.2958)
Weisz D. R., Johnson B. D., Conroy C., 2014, preprint (arXiv:1409.4772)
Wilkins S. M., Bunker A. J., Ellis R. S., Stark D., Stanway E. R., Chiu K., Lorenzoni S., Jarvis M. J., 2010, MNRAS, 403, 938
Windhorst R. A., Cohen S. H., Jansen R. A., Conselice C., Yan H., 2006, New A Rev., 50, 113
Yan H., Windhorst R. A., 2004, ApJ, 612, L93
Yan H., et al., 2011, ApJ, 728, L22
Yan H., et al., 2012, ApJ, 761, 177
Zheng Z.-Y., et al., 2013, MNRAS, 431, 3589
van Breukelen C., Jarvis M. J., Venemans B. P., 2005, MNRAS, 359, 895

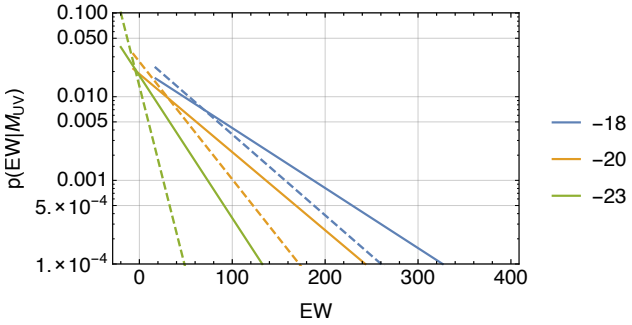

Figure A1. The PDF $P(EW|M_{\rm UV,}{}_z)$ as described in Eq. (3) for three different values of $M_{\rm UV}$. The solid (dashed) lines shows the EW distribution for $z = 5.7$ ($z = 3.1$). Negative EWs corresponds to having Lyα in absorption. Note that for about half of $z \sim 3$ LBGs, Lyα is seen in absorption (Shapley et al. 2003). Our formalism incorporates this measurement (see Dijkstra & Wyithe 2012).

APPENDIX A: VARYING THE EW DISTRIBUTION

In this appendix, we demonstrated that our main results and conclusions do not depend on our assumed EW-PDF.

A1 Fiducial $P(EW)$

Our default EW distribution is given by Eq. (3). We plot the PDF for three UV magnitudes and two redshifts in Fig. A1.

A2 Schenker et al. (2014) parameterization

As mentioned in Sec. 2, Schenker et al. (2014) suggest an alternative parameterization of the EW-PDF, namely

$$P(EW|\beta) = \frac{A_{\rm em}}{\sqrt{2\pi}\sigma EW} \exp\left[-\frac{(\log EW - \mu(\beta))^2}{2\sigma^2}\right] . \quad \text{(A1)}$$

This log-normal PDF possesses the parameters $A_{\rm em}$, σ and μ. The latter is given by

$$\mu(\beta) = \mu_\alpha + \mu_s(\beta - 2.0), \quad \text{(A2)}$$

where β is the UV continuum slope. Schenker et al. (2014) found their EW distribution to depend more strongly on β than on $(M_{\rm UV}, z)$, and therefore constrained $P(EW|\beta)$. We can include this parameterization into our formalism if we map $P(EW|\beta)$ onto $P(EW|M_{\rm UV}, z)$.

This mapping is based on three results from Bouwens et al. (2014b):

(i) We use their empirical linear correlation between $\beta - M_{\rm UV}$ at $z \sim 7$. This relation constrains $\beta(M_{\rm UV} = -19.5) = -2.05 \pm 0.09 \pm 0.13$.
(ii) Furthermore, we apply their measured change per unit redshift $\Delta\beta/\Delta z = -0.1 \pm 0.05$.
(iii) Finally, we use their measurement that $\Delta\beta/\Delta M_{\rm UV} = -0.2$ (-0.08) for $M_{\rm UV} \leqslant -19$ (> -19).

Accordingly, our mapping can be written as

$$\beta = \beta_0 + \mu^{(\beta)}_{M_{\rm UV}}(M_{\rm UV} + 19) + \mu^{(\beta)}_z(z - 7), \quad \text{(A3)}$$

where $\mu^{(\beta)}_{M_{\rm UV}} \equiv \Delta\beta/\Delta M_{\rm UV}$ and $\mu^{(\beta)}_z \equiv \Delta\beta/\Delta z$.

In Eq. (A1) we used the best parameters by Schenker et al. (2014), i.e., $(A_{\rm em}, \sigma, \mu_\alpha, \mu_s) = (1.0, 1.3\,, 2.875, -1.125)$. In addition, since $A_{\rm em}$ is degenerate with F, we set $F = 1$. The orange dashed line in Fig. A2 shows the resulting Lyα LF at $z = 5.7$. The agreement in the faint-end between the two procedures is remarkable. For greater luminosities, however, the Schenker et al. (2014) parameterization leads to a (much) higher number density of LAEs. While there are significant uncertainties in the above procedure, the agreement we get at the faint end slope is especially encouraging. Future surveys can be extremely useful in further connecting the LAE and LBG populations by constraining the bright end of the LAE luminosity function.

A3 'Freezing' the EW PDF for faint galaxies

Since the evolution in the EW PDF for fainter sources involves a (modest) extrapolation of observationally inferred $P(EW)$, we have also tested and alternative PDF where we 'froze' the evolution at $M_{\rm UV} = -19$. That is, we also conservatively assume that the EW-PDF stops evolving at $M_{UV} > -19$ (even though observations hint that this is not the case, see fig. 13 of Stark et al. (2010)). Fig. A2 shows the resulting Lyα LF (purple line). It is clear that our results are only affected slightly, i.e., the faint-end-slope $\alpha_{{\rm Ly}\alpha}$ is reduced by ~ 0.05. We also tested this over a variety of redshifts.

A4 Non-constant UV spectral slope

The spectral slope β is not a constant, but depends on UV magnitude and redshift (as discussed above). This introduces some additional dispersion in the predicted Lyα flux at a fixed $M_{\rm UV}$. However, varying β within $[-2.0, -1.5]$ changes the Lyα flux only by $1 - (\lambda_{\rm UV}/\lambda_{{\rm Ly}\alpha})^{1.5-2.0} \sim 13\%$. This dispersion is smaller than that introduced by the EW-PDF. If we replace the constant β with the empirical fit described in § A2, then our predicted Lyα LF (represented by the *orange line* in Fig. A2) is barely any different from our fiducial model that used $\beta = -1.7$ (represented by the *black solid line*).

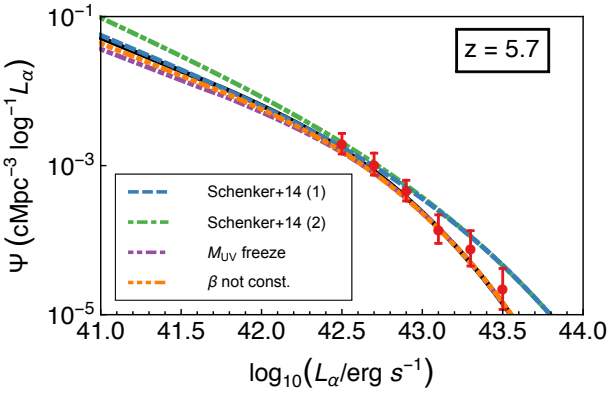

Figure A2. The Lyα LF at $z = 5.7$ for different EW distributions. The solid black line and Ouchi et al. (2008) data points are the same as shown in Fig. 1. As comparison we show the Lyα LF computed using the Schenker et al. (2014) parameterization of the EW PDF once with the full $\beta - M_{\rm UV}$ relation as given in § A2 (blue dashed line) and once with a constant $\mu^{(\beta)}_{M_{\rm UV}} = -0.2$ over all $M_{\rm UV}$ (green dashed-dotted line). Also shown are our results when freezing the EW PDF at $M_{\rm UV} = -19$ (purple) and when using the $\beta - M_{\rm UV}$ relation instead of a constant β (orange).